Incorporation and localisation of alkanes in a protomembrane model

Loreto Misuraca, Josephine Loricco, Philippe Oger, Judith Peters, Bruno Demé

Alkane localisation inside a compliant protomembrane model

Loreto Misuraca[a,b], Josephine LoRicco[c], Philippe Oger[c], Judith Peters[a,b,d,*], Bruno Demé[b,*]

[a] Univ. Grenoble Alpes, CNRS, LIPhy, 38000 Grenoble, France.
[b] Institut Laue Langevin, F-38042 Grenoble Cedex 9, France
[c] INSA Lyon, Université de Lyon, CNRS, UMR5240, Villeurbanne, France.
[d] Institut Universitaire de France.

*Corresponding authors : Judith Peters, jpeters@ill.fr and Bruno Demé, deme@ill.fr

Abstract

Protomembranes at the origin of life were likely composed of short-chain lipids, readily available on the early Earth. On the other hand, membranes formed by such lipids are less stable and more permeable under extreme conditions, so that a novel membrane architecture was suggested to validate the accuracy of this assumption. The model membrane includes the presence of a layer of alkanes in the mid-plane of the protomembrane in between the two monolayer leaflets and lying perpendicular to the lipid acyl chains. Here, we investigated such possibility experimentally for membranes formed by the short-chain phospholipid 1,2-didecanoyl-*sn*-glycero-3-phophocholine, including or not the alkanes eicosane, squalane or triacontane by means of neutron membrane diffraction and contrast variation. We found strong indications for an incorporation of two of the three alkanes in the membrane mid-plane through the determination of neutron scattering length density profiles and the membrane swelling at various relative humidities indicating a slightly increased bilayer thickness when the alkanes are incorporated into the bilayers. The selectivity of the incorporation points out the role of the length of the n-alkanes with respect to the capacity of the membrane to incorporate them.

Introduction

The cell membrane is among the most fascinating macromolecular structures that make up all living systems. It is a biological, mainly two-dimensional matrix that separates and protects the interior of the cell from its environment. The basic unit of cell membranes (which generally consist of lipids, proteins and carbohydrates) is a bilayer of polar lipids (phospholipids, glycolipids) whose polar head-groups point outwards and stabilize the bilayer, while the hydrophobic acyl chains constitute the membrane core. Biomembranes promote the compartmentalization of living systems, which is an essential property for the definition of life. This fact probably played a key role in the early stages of the formation of the first membranes and thus in the origin of life on our planet [1-5].

Several structural studies have been performed on lipid membranes to obtain quantitative information on their molecular organization, phase transitions and phase separations, incorporation and effects of host molecules and macromolecules [6], etc. These structural characterizations are often complicated by the fact that the biologically relevant phases are not crystalline, therefore there is no three-dimensional repeat unit that can be resolved through usual crystallographic methods. Instead, lipids typically arrange into liquid-crystalline phases, e.g. gel (L_β, P_β) or fluid (L_α) lamellar phases, which possess intrinsic static and/or dynamic lateral disorder. X-ray and neutron diffraction techniques have been important tools in this respect, because they allow one-dimensional information of the membrane ordering to

be obtained both in the bilayer plane and perpendicular to it, despite the lateral disorder of the various lamellar phases precisely when in the biologically relevant (L_α) fluid phase.

From seminal studies performed back in the 1970s [7-10], a methodology was developed to extract the neutron and x-ray scattering length density (SLD) profiles of membranes from solid-supported stacks of parallel membranes opening the field known today as *membrane diffraction*. The analysis of the SLD profiles gives information on the average positioning and dimensions of each membrane constituent [11]: hydrocarbon chains, headgroup components (e.g. the phosphate and the choline groups) [12, 13], water and additional incorporated host molecules, when present (e.g. cholesterol) [8, 9].

With this quantitative information at hand, one can investigate the location of intercalants within the membrane and correlate it with the observed consequences on the membrane structure, as well as its properties and functioning. This was done, for example, by using n-alkanes of varying chain length to investigate the mechanisms of anaesthesia [14, 15]. These studies proved that a significant amount of n-alkanes (e.g. hexane [16]) entered the bilayer core, although the resolution was not sufficient to determine whether there was a preferential positioning (i.e. sitting parallel or perpendicular to the lipid acyl chains). Another study [17] was performed using high amounts of C6 – C16 n-alkanes (0.3 – 0.9 alkane:lipid ratio) on egg PC membranes, finding that smaller n-alkane chain lengths contributed to an increase in bilayer thickness. More recently, the exact positioning of small amounts of squalane (branched C30 alkane) was determined in model membranes made of DOPC:DOPG [18] and an archaea-mimicking mixture DOPhPC:DOPhPE [19]. In both cases, squalane was found to enter the lipid membrane and to position in the mid-plane of the bilayers perpendicularly to the lipid tails. Such novel membrane architecture was suggested earlier by Cario et al. [20] and then confirmed experimentally. Moreover, the two studies highlighted the possibilities for the incorporated molecules to act as proton permeability barrier [18] and to trigger domain formation [19].

In analogy with previous findings, our group has studied the incorporation of n-alkanes in early life membrane models composed of short single chain amphiphiles (SCAs) with 10-carbon (C10) chain length [21]. The reason for this lies in the likely presence of a broad size distribution of n-alkanes (especially linear ones) along with SCAs in the early Earth environment, as both species are readily formed via Fischer-Tropsch type reactions [22, 23]. If a structural role could be identified for such apolar molecules into the prebiotic membranes, this would help explain how SCA membranes could have withstood the harsh environmental conditions of the early planet. In our recent study [21], we found that the alkanes squalane and eicosane (C20 linear) decrease the temperature induced membrane swelling of multilamellar vesicles (MLVs) and decrease the membrane sensitivity at high hydrostatic pressure. These results show that the incorporation of n-alkanes can indeed confer a higher membrane stability at high temperatures and pressures and therefore could have played a major role in the formation of the first forms of life.

It is now important to determine the actual positioning of such molecules inside short-chain lipid membranes. First, the existence of a preferential orientation of the alkanes inside the membrane could help gain insight into the mechanisms by which the bilayers acquire a higher thermo- and piezo-stability. Second, it might explain the need for more or less intercalant in order to obtain significant effects in the membrane (for instance, an orientation of the alkanes perpendicular to the acyl chains might correlate with very small amounts needed in the membrane). Third, the positioning may affect membrane structural features, e.g. the bilayer thickness, possibly offering a way to obtain a thicker membrane even in conditions where only short chain lipids are available.

Previous structural studies on model membranes have focused on lipids having chain length of 12 carbons or longer [12, 13, 24]. Here, we performed our investigation using the C10 PC lipid 1,2-didecanoyl-*sn*-glycero-3-phosphocholine (hereafter DCPC, Figure 1a) as phosphocholine C10 analogue of the previously studied SCA membranes [21, 25]. This allows to benefit from optimized procedures for successfully producing membrane stacks onto silicon substrates [12], which are needed for obtaining structural information by membrane diffraction. We combined two approaches to neutron diffraction studies, contrast variation and membrane swelling (see Materials and Methods section), to fully characterize DCPC bilayers in the absence or presence of small amounts of three alkanes: eicosane (Figure 1b), squalane (Figure 1c) and triacontane (C30 linear, Figure 1d).

We found that the alkanes eicosane and squalane enter the membrane hydrophobic core and lead to an increase of the bilayer thickness compared to the alkane-free sample. Conversely, the triacontane does not lead to an increase in membrane thickness, hence questioning its incorporation into the membrane and suggesting a role of the n-alkane length for a successful inclusion in the bilayer.

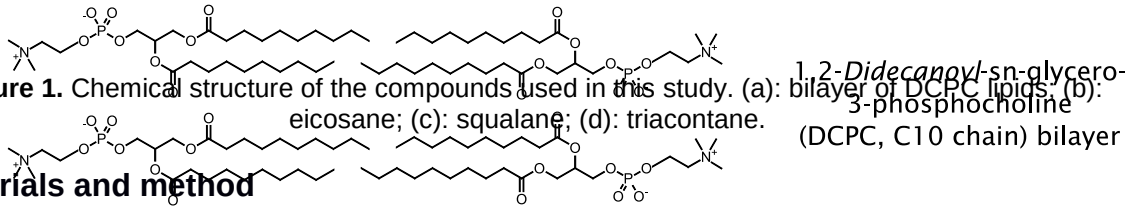

Figure 1. Chemical structure of the compounds used in this study. (a): bilayer of DCPC lipids; (b): eicosane; (c): squalane; (d): triacontane.

Materials and method

1. Sample preparation

DCPC was purchased from Avanti Polar Lipids (Alabaster, AL, USA). Hydrogenated and perdeuterated eicosane, squalane and triacontane were purchased from Sigma Aldrich (Merck, Darmstadt, Germany). All products were used as received from the manufacturer, without further purification. 5 mg of DCPC or DCPC with 4% molar of the corresponding hydrogenated or deuterated alkane (eicosane, squalane or triacontane) were dissolved in chloroform:methanol (2:1), spread on a silicon wafer (Si-Mat., Kaufering, Germany) using the "rock and roll" method [26] and dried overnight under vacuum. Next, the samples were placed in sealed Falcon tubes containing about 100 µL of H_2O at 40 °C for 24 hours of annealing. Finally, samples were stored at ambient temperature before the experiments.

2. Neutron Diffraction experiments

Neutron diffraction experiments were performed at the D16 neutron diffractometer [27] at the Institut Laue - Langevin (ILL, Grenoble, France). The incident wavelength was 4.46 Å. The position sensitive Millimeter resolution Large Area Neutron Detector (MiLAND, 320 x 320 mm^2 with 1 x 1 mm pixel resolution) was set to a sample-to-detector distance of 950 mm. Sample rocking scans (Ω-scans) were used to collect neutron diffraction data in reflection geometry by scanning the sample angle with respect to the incident beam (Ω) using 0.05° increments at two detector angles Γ relative to the incident neutron beam, Γ = 12° (-1 < Ω < 12°) and Γ = 28° (8 < Ω < 18°) in order to collect the maximum number of diffraction orders (Figure 2). The resulting q-range investigated was q = 0.06 $Å^{-1}$ - 0.86 $Å^{-1}$, where q is the neutron scattering vector. Diffraction experiments were performed using a set of three identical [28] humidity chambers (BerILL) developed at ILL, allowing for precise control of the humidity and the temperature. The temperature at the sample position was kept at the constant value of T = 25°C. The relative humidity (RH) was precisely regulated by the temperature difference between the sample and the water reservoir controlled independently

using a dedicated controller for the chambers and a Lakeshore 336 (Lake Shore Cryotronics, Inc., Westerville, OH, USA) for the readout of the high-precision temperature sensors [28].

The DCPC samples, pure or containing 4% of either hydrogenated or deuterated alkanes, were measured following two different procedures. In the first (*contrast variation experiments*), samples were incubated at a constant RH of 97% for 2 hours before starting each scan. Every sample was incubated three times inside the humidity chamber at different D_2O contrasts, with the reservoir filled with 20 ml of different mixtures of D_2O/H_2O (8%, 70% or 100%). The different contrasts were used to extract the phase of each Bragg reflection required to determine the membrane neutron scattering length density (NSLD) profile [8].

In the second experimental procedure (*swelling experiments*), the D_2O/H_2O solvent contrast was set to a zero NSLD obtained using the 8% D_2O mixture. Here, the RH was varied from 30% up to ≈ 100% in order to scan the sample lamellar periodicity and Bragg reflection intensities as a function of humidity from a dehydrated state up to full hydration. Sample equilibration was gradually increased from 1 hour (used for the lowest humidity steps) up to 2.5 hours for the sample equilibrated at 99.5% RH. For the last measurement aimed at reaching full hydration, samples were equilibrated offline for 24 hours in the measurement chamber.

An example of reciprocal space map obtained by merging two Ω-scans is shown in Figure 2. The first visible feature is the occurrence of a series of reflections located at the same periodicity (q_z) on top of the line $q_{//} = (q)/2$ that corresponds to the specular condition. The periodicity identified by the reflections results from the lamellar ordering of the multilayer, with a repeat or center-to-center distance given by one bilayer plus one water layer. Each reflection does not have the shape of a Bragg peak as expected from a perfect crystal, but that of a Bragg sheet in the vertical ($q_{//}$) direction, due to fluctuations and defects in the liquid crystal's organization.

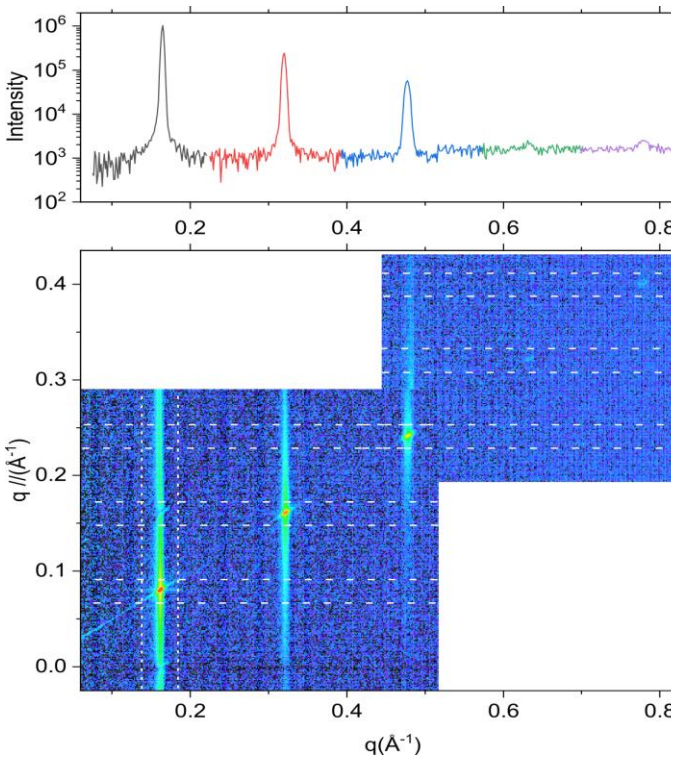

Figure 2. Example of reciprocal space map ($q_{//}$ vs q) of DCPC at 8% D_2O contrast and 30% relative humidity showing 5 lamellar diffraction orders. Horizontal white dashed lines show the limits of

integration for each diffraction order, while the top plot shows the result of the integrations truncated in the selected Ω and 2θ regions of interest for the peak fitting.

These elongated features are a sign of the disorder both static or dynamic of the membrane stack. Two minima lines can be observed from the 2D map, one that is located at constant Ω = 0 and the other tracing the line Ω = 2θ. These minima correspond to the so-called *sample horizons*, and occur at the angles where the scattered beam is attenuated by crossing longitudinally the lamellar stack on the silicon substrate.

1. Data reduction

Data reduction was performed using the ILL software LAMP [29]. Pixel efficiency as well as solid angle corrections were performed using a detector calibration obtained from the flat incoherent scattering signal of a water measurement. The background was obtained by collecting an empty humidity chamber scan and was subtracted from each measurement. The background-subtracted data were then exported for further analysis using Origin Pro (Version 2019, OriginLab Corporation, Northampton, MA, USA). The data were reduced to 1D intensities vs 2θ plots by integrating for each peak a slice of Ω = 1° width around the peak center (see Figure 2).

The integrated intensities of the Bragg peaks were obtained using Gaussian fits, as done previously [30]. The angle (θ) of a Bragg peak is related to the scattering vector (q) by:

$$q = \frac{4\pi sin(\theta)}{\lambda} \quad (1)$$

where λ is the wavelength of the incident neutron beam. The periodicity (*d-spacing*) was derived as in references [31, 32]. For each sample and experimental condition, a weighted linear fit was performed on a plot of peak positions (in q) as a function of the diffraction order (h) (known as *Bragg plot*), the slope (s) of which was used to determine the *d-spacing* via the equation:

$$d = \frac{2\pi}{s}. \quad (2)$$

The error on the *d-spacing* was obtained by propagating the error of the peak position fitting and used in the weighted linear fit to the peak positions *vs*. Bragg order *h*.

The next step in the data analysis is to convert reciprocal space data into real space 1D structures. For that, the calculated area of each peak was employed to construct neutron scattering length density (NSLD) profiles from the sum of the neutron scattering lengths per unit volume [33]. The way the membrane stack NSLD profiles can be constructed comes from the definition of the scattering intensity I(q) as:

$$I(q) = P(q) * S(q) \quad (3)$$

where P(q), the membrane form factor, contains information about the repeat unit structure (in our case, one bilayer and one water layer) while S(q), the structure factor, is related to the spatial correlation between adjacent membranes that results from their interactions and leads to the lamellar periodicity and to the Bragg reflections. Therefore, the S(q) features (the Bragg peaks) are modulated by the underlying form factor, and this property can be used to sample the form factor dependence with q at discrete positions exploiting the intensity modulation of all Bragg reflections that are observed in a sample scan [7-9]. The Fourier transform of P(q) in real space provides the NSLD profiles.

In practice, since one only has access to a finite number of q positions through the Bragg reflections, approximated NSLD profiles are calculated from the discrete set of Fourier

coefficients F_h (also referred as "structure factors" in the text) using the following equation [7, 8, 10]:

$$\rho(z) = \sum_{h=1}^{h_{max}} |F_h| v_h cos\left(\frac{2\pi h}{d} z\right) \quad (4)$$

where d is the lamellar periodicity of the bilayer stack in the z direction perpendicular to the membrane plane, $|F_h| = \pm\sqrt{I_h h}$ where I_h is the integrated intensity of the h^{th} order Bragg peak and v_h is the phase of the structure factor terms that are in general complex quantities including information on absorption and activation of the sample [34]. However, in the case of centrosymmetric structures such as bilayers, $v_h = \pm 1$ and the phase assignment simplifies into the assignment of a + or - sign for each F_h term [8].

Finally, from the data acquired by scanning the RH (swelling experiments), the osmotic pressure (Π) [35, 36] could be calculated from the relative humidity using the following equation:

$$\Pi = \frac{-k_B T}{v_w^0} ln\,(RH) \quad (5)$$

where RH is defined as P/P_0 (e.g. 0.5 for 50% RH), k_B is Boltzmann's constant, T is the temperature in Kelvin, and v_w^0 is the molecular volume of water [31].

2. Scattering Length Density profile determination

In order to gather insights about the membrane structural changes, the first step was to extract the corresponding NSLD profiles of each sample. This was done by exploiting the modulation in the intensity of each membrane Structure Factor term $F_h(q)$ as detailed in the "Data reduction" section. The main challenge relies in the assignment of the phase which, in the case of centrosymmetric structures such as membrane stacks, simplifies into the assignment of a positive or negative sign to each term. In this work, we combined three strategies to obtain an unambiguous phase assignment:

1. Contrast variation: the use of different D_2O / H_2O isotopic compositions allows to vary the water NSLD that is the contrast between bilayers and water layers. By using the fact that the NSLD of water increases linearly with the D_2O percentage, one can detect the occurrence of phase changes.

2. Swelling: when the RH of the environment increases, the membrane stack undergoes swelling, as a result of the hydration and the increase of the water layer thickness. Assuming that the bilayer structure does not change when the water layer increases, one can perform Relative Humidity (RH) scans and use the displacement in q of the Bragg reflections to sample the P(q) in a finite set of q positions [8]. With this technique, one obtains information on the possible sign swapping whenever the tracing of the P(q) vs q highlights the presence of a relative minimum.

3. Physical considerations from the observed NSLD profiles: as highlighted in the former points, the contrast variation and swelling techniques both allow detection of phase changes, but not the absolute phases. However, the features of the NSLD profiles can be qualitatively judged from our knowledge of the system. For instance, the acyl chains placed in the middle of the bilayer should give a broad minimum in the profile because of the high density of low scattering length hydrogen atoms. Conversely, the phosphate groups of the phosphatidylcholines (the DCPC

headgroups) give local maxima that will be highly visible at the lowest water contrast of 8% D_2O. In addition, different D_2O contrasts at a constant RH do not change the shape of the NSLD in the hydrocarbon region. Similar considerations were also made when applying scaling and offset factors to the NSLD profiles to allow for comparisons between different samples: there, the NSLD profiles of the different samples were matched with each other in the solvent region, for the measurements performed at the same D_2O / H_2O contrast.

Results

Figure 3 shows examples of the resulting contrast variation plots for the DCPC samples with and without perdeuterated eicosane or squalane molecules. All numerical values of the structure factor terms and the measured d-spacing can be found in Table 1 in the Electronic Supplementary Information (ESI).

The choice of the sign for the 1st reflection order, the term which is a function of the overall periodicity of the repeat unit (the d-spacing), is assigned as negative in order to obtain a local minimum of the NSLD profiles at the z = 0 position (Figure 4). This translates into the choice of setting the centre of the bilayer repeat unit at the 0 of the x-axis. All other phases were assigned by making sure that, in the following order:

1) the linearity in the contrast variation plots was maintained (Figure 3);

2) combining the shape observation of the NSLD profiles at all 3 contrasts;

3) applying the phase change when needed (in our case, for the 3rd Bragg reflection order around 70% D_2O/H_2O, visible in Figure 3).

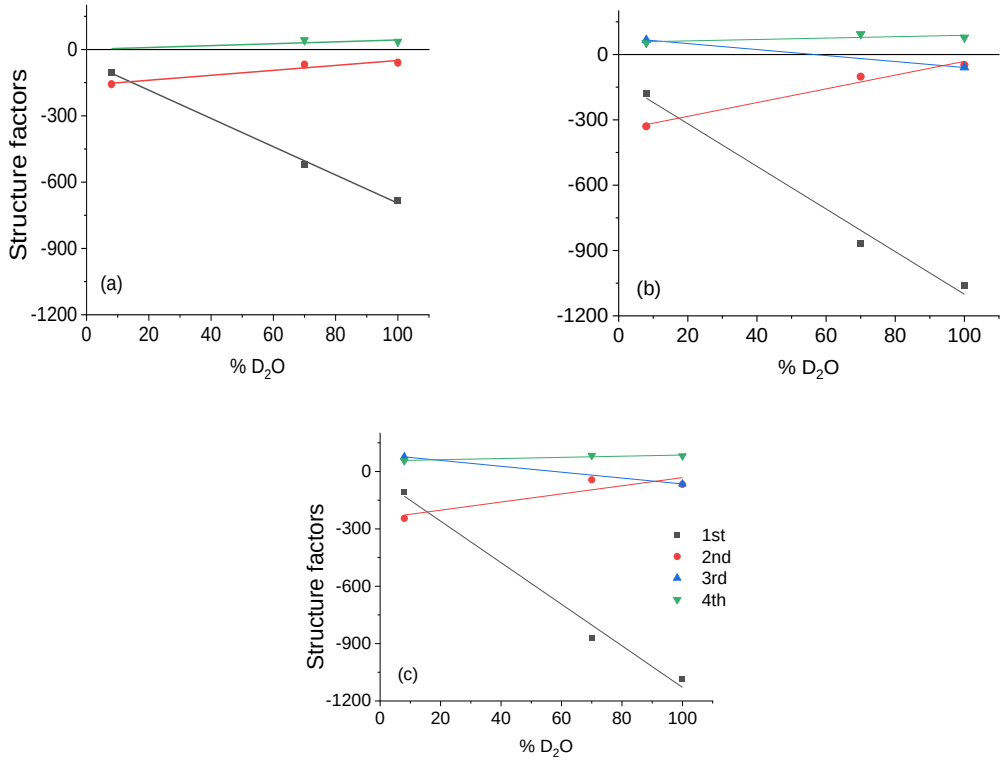

Figure 3. Examples of contrast variation plots for the DCPC samples with and without added alkanes. (a) DCPC. (b) DCPC + 4% d-eicosane. (c) DCPC + 4% d-squalane.

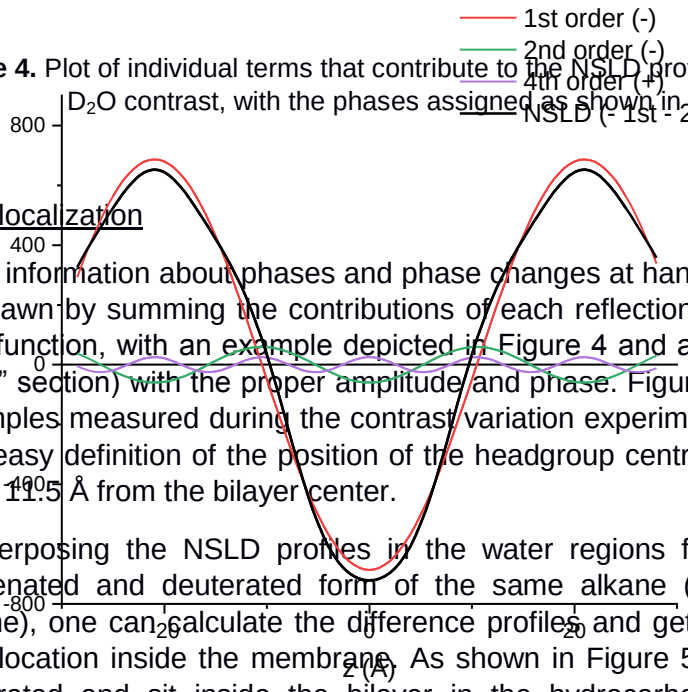

Figure 4. Plot of individual terms that contribute to the NSLD profile of the DCPC sample at 100% D_2O contrast, with the phases assigned as shown in panel (a) of Figure 3.

Alkane localization

With all information about phases and phase changes at hand, the membrane NSLD profiles were drawn by summing the contributions of each reflection order (all having the form of a cosine function, with an example depicted in Figure 4 and as detailed in the "Materials and Method" section) with the proper amplitude and phase. Figure 5 shows the NSLD profiles of the samples measured during the contrast variation experiments at 8% D_2O/H_2O contrast. It allows easy definition of the position of the headgroup centres, at the local maxima located at $z \approx \pm 11.5$ Å from the bilayer center.

By superposing the NSLD profiles in the water regions for the samples containing the hydrogenated and deuterated form of the same alkane (h- and d-eicosane; h- and d-squalane), one can calculate the difference profiles and get information about the average alkane location inside the membrane. As shown in Figure 5, both alkanes are found to be incorporated and sit inside the bilayer in the hydrocarbon region, preferentially in the midplane in between the monolayers.

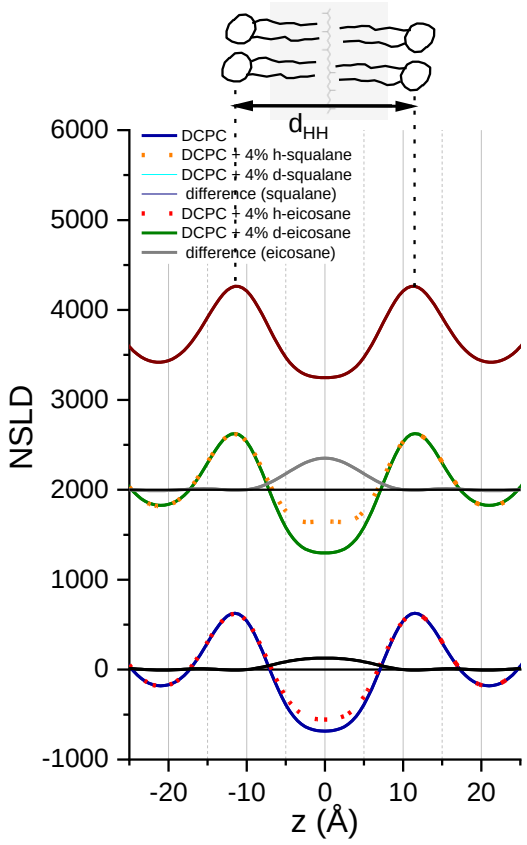

Figure 5. NSLD profiles at 8% D_2O contrast of samples measured at 97% RH. The y-axis scale refers to the alkane containing samples, while the other NSLD profiles were shifted for clarity. The top image shows a sketch of the bilayer whith a molecule of squalane in the mid-plane, as mapped by the NSLD profiles within the dotted lines defined by d_{HH} the position of the maxima.

Membrane swelling

In addition to screening the phase of the membrane structure factors as a function of humidity, swelling experiments (at 8% D_2O contrast, to easily locate the lipid headgroup position) provided further information on the membrane characteristics and properties. The samples measured here were a) DCPC; b) DCPC + 4% h-eicosane; c) DCPC + 4% h-squalane; d) DCPC + 4% h-triacontane. All numerical values of the structure factor terms can be found in Table 2 in the ESI. Figure 6 shows an example of the NSLD profiles obtained at each measured RH for the DCPC sample. Some qualitative features are visible from the plot:

- The lowest humidity values of 30% and 50% show a more pronounced minimum in the centre of the bilayer. This can be attributed to the higher density of hydrogen atoms at the terminal methyl group position, a feature that disappears at higher humidity values presumably because of an increase in membrane static and/or dynamic disorder.
- The repeat distance (d-spacing) increases with increasing RH, as expected because of the water layer thickening between bilayers.
- The bilayer thickness decreases with increasing RH, shown in the plot as a shift of the headgroup maxima position.

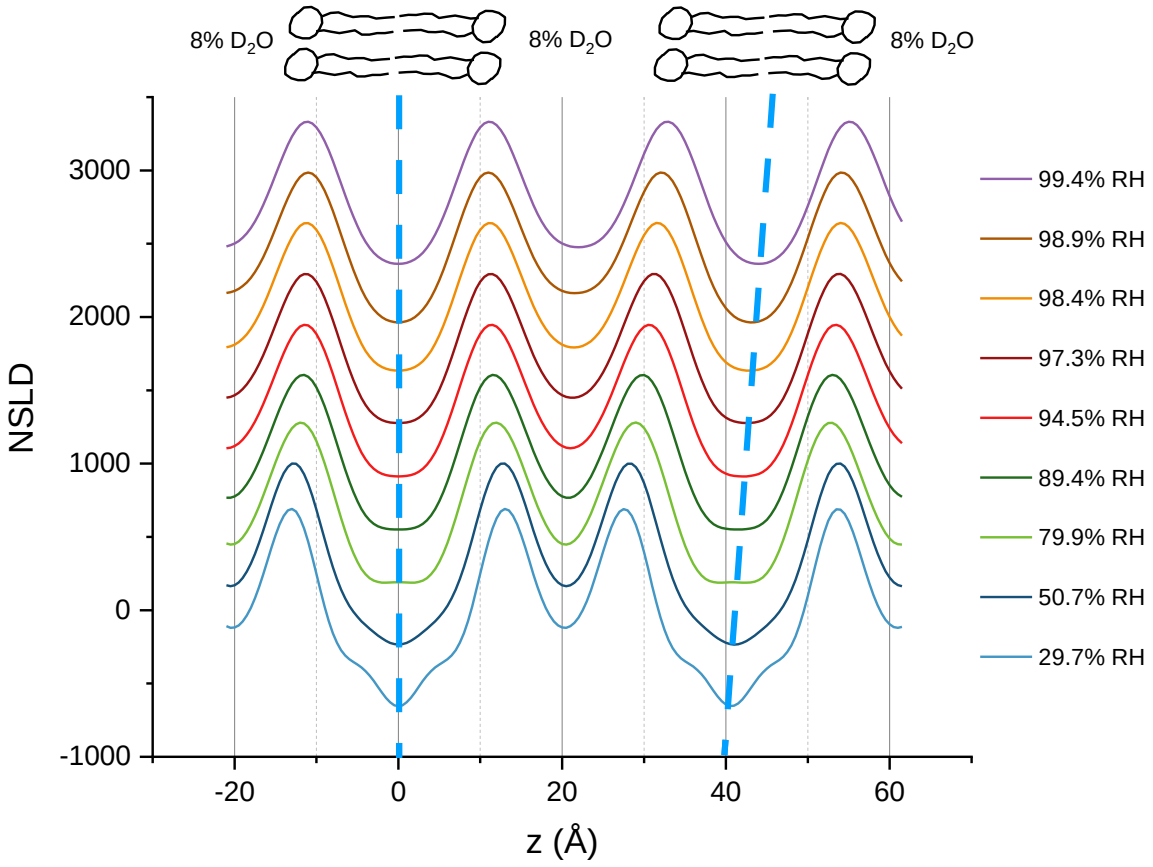

Figure 6. NSLD profiles of a DCPC sample during swelling experiments showing 2 unit cells. The blue dotted lines show a perfect vertical line as reference on the left side and the effect of swelling with a minimum shifted more and more to the right side. Top image represents the location of the two bilayers mapped by the NSLD profiles. Water contrast was 8% D_2O.

The last two features can be used for quantitative comparison between the different samples investigated. Figure S1 in the ESI shows the bilayer thickness changes as a function of humidity for all samples. We use here the same nomenclature applied in former diffraction studies carried out on DLPC and DMPC samples [12]. As a first definition of the bilayer thickness, we define d_{HH} as the distance between the two maxima in the NSLD profiles at 8% D_2O contrast, that corresponds to the distance between the phosphate groups of the PC.

As shown in figure S1, d_{HH} decreases for all samples when humidity increases. Interestingly, the membrane thickness of the samples containing eicosane and squalane appears to be offset by a value of approximately [0.5 – 1] Å, while this is not observed for the sample containing triacontane. The lipid molecular volume (V) being constant, the decrease in bilayer thickness (d_{HH} = 2l where l is the lipid length), is consistent with an increase of the area per headgroup (A) upon increasing hydration, according to:

$$A = \frac{V}{l}. \quad (6)$$

From previous data on DMPC and DLPC [12], since the headgroup area should not change significantly between DMPC, DLPC and DCPC, we assume an average area A ≈ 62 $Å^2$ between the reported values [12] A = 60.6 $Å^2$ (DMPC) and 63.2 $Å^2$ (DLPC). Also, considering the lipid volume V_L scaling linearly with the chain length (V_L = 1101 and 991 $Å^3$ for DMPC and DLPC, respectively), we obtain V_L ≈ 881 $Å^3$ and a calculated d_{HH} ≈ 20.3 Å for DCPC at full hydration. As our reported value at maximum hydration is $d_{HH} \simeq 22.5 \pm 0.5$ Å, this result suggests that the DCPC membranes at the highest measured RH were close to full hydration, but not fully hydrated, (Figure S1).

The feature of interest, namely the water layer thickness as a function of humidity, is shown in the more common pressure – distance plot in Figure 7. In order to estimate the water layer thickness $d_{w'}$, we used existing data from the literature on PC lipids to estimate the thickness of the headgroups [12]. This led to the following formula for our calculation of $d_{w'}$:

$$d_{w'} = d - d_{b'} = d - d_{HH} - 8.1 \text{ Å}. \quad (6)$$

where $d_{b'}$ is the bilayer thickness calculated from the interfaces water-headgroup.

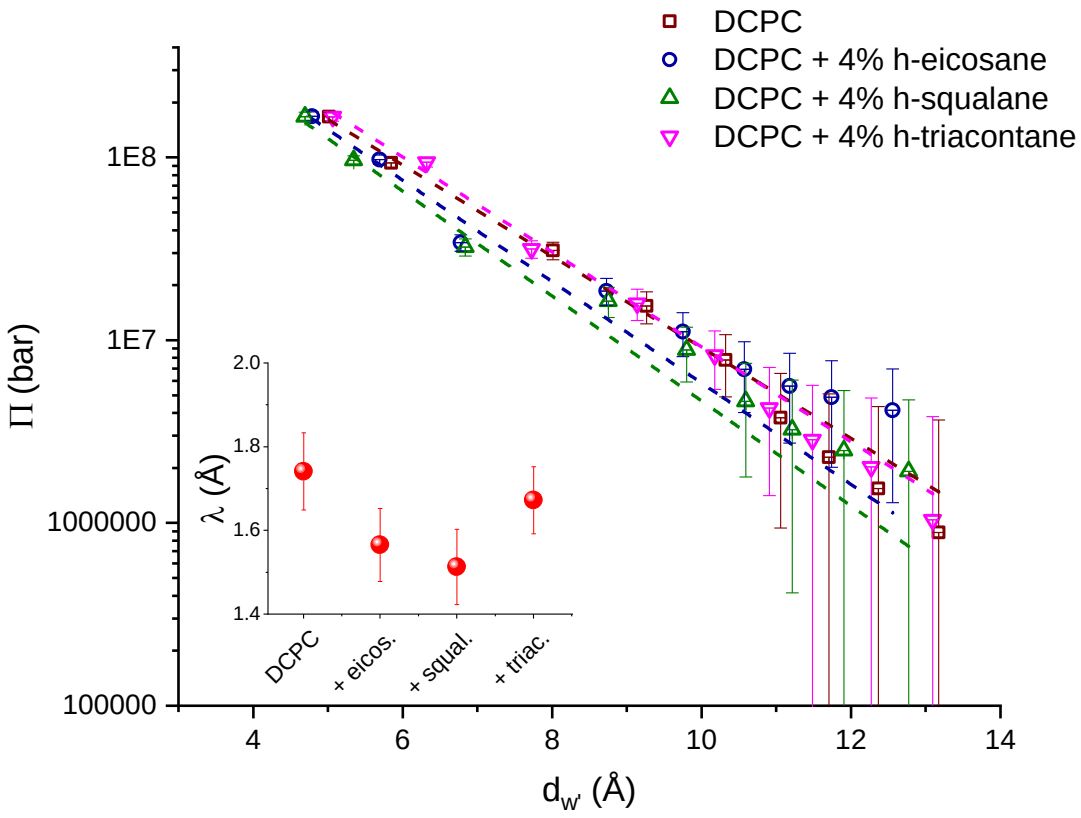

Figure 7. Pressure-distance curves: osmotic pressure Π as a function of the water layer thickness $d_{w'}$ calculated for all samples. Inset: decay lengths found from exponential fits for the four samples.

The data show very small qualitative differences probably due to the humidity range explored, still far away from the expected values for maximum swelling in bulk with excess water (the water layer thickness at full swelling for PC lipids is known to be at $d_{w'} \approx$ 20-22 Å [12] and the bilayer thickness did not shrink to the expected minimum value, as previously reported). Exponential fits of Π as a function of $d_{w'}$ yield an estimation of the decay length λ (inset of Figure 7). Although the differences are small, the samples containing eicosane and squalane show slightly lower decay lengths which could imply a lower swelling limit for these two samples. The obtained λ values are slightly lower than the value reported in the literature for DLPC membranes (around λ = 2.1 Å) [37].

Discussion

Our results allow us to gain numerous insights regarding the structure of a short chain membrane model, with and without insertion of additional apolar molecules (linear and branched alkanes).

First, contrast variation measurements clearly show that both the alkanes, eicosane and squalane, are included in the hydrocarbon region of the DCPC bilayer (Figure 5). Compared to earlier studies by Hauss et al. [18] and Salvador-Castell et al. [38], we find an alkane layer of almost identical size, so that we can conclude that the alkanes are likely oriented perpendicular to the lipid acyl chains. In addition, the bilayer thickness values calculated from fitting the maxima of the NSLD profiles at 8% D_2O contrast (Figure S1) show an offset of ≈ 0.5 - 1 Å compared to the alkane-free DCPC membrane, confirming further the incorporation of the alkanes in the mid-plane.

Such finding is of primary importance for the protomembrane model suggested here. A similar strategy was forwarded already for modern membranes in archaeal cells, which

withstand the most extreme conditions. We found a similar architecture and investigated in many details the consequences of the presence of the apolar lipids [19, 38]. In particular, they are able to extend the stability domain, to reduce the membrane's permeability to protons but to increase that of water, and to induce a negative curvature in the membrane, allowing the transition to novel non-lamellar phases. As these characteristics are mandatory for the good functioning of the membrane in extreme conditions, they can be taken as indicative for the architecture of protomembranes, and we found already positive impact of alkanes on the stability of protomembranes under high temperature and pressure conditions [39, 40] and on their molecular dynamics [41]. In this context the experimental proof of the presence of the apolar lipids is an important step.

Interestingly, a slight increase of the bilayer thickness offset with humidity increase (differences in Figure S1) might suggest a small effect of the hydration in increasing the portion of alkane molecules accommodating in the mid-plane normal to the bilayer plane. The thickness offset is not observed on the sample containing triacontane, which suggests that it is not included in the bilayer and that size might play a role in the ability of such molecules to be successfully inserted within the bilayer. The long-axis length of eicosane (C20) and squalane (C30) being similar (because of the branched structure of the squalane) and of the same order of twice the lipid chain length of DCPC are capable of inserting within the membrane, however the triacontane size could not be accommodated in the hydrocarbon region by intercalating parallel to the lipid chains (see Figure 1). Perhaps due to the need for the membrane to assume a certain undulated in-plane arrangement (governed by the lipid intrinsic geometry and the membrane bending/compression moduli), the arrangement of triacontane perpendicular to the lipid chain is not possible, so that these molecules are excluded from the membrane and are not observed in the calculated NSLD profiles. Such a conclusion remains, however, speculative.

All membrane stacks investigated show a clear effect of the humidity increase in thinning the bilayer up to ≈ 4 Å in the humidity range ≈ 30 - 100%, which is consistent with the increase of the headgroup area observed in PC lipids of longer chain lengths [12]. The extent of such decrease in bilayer thickness is not affected by the inclusion of alkane molecules. The decay length of the samples containing eicosane and squalane is slightly lower than than that of pure DCPC, implying a possible lower swelling limit induced by the alkane presence. The compatible value of λ between DCPC and DCPC + triacontane samples gives an additional indication that the latter alkane did not incorporate into the membrane.

To summarize, we have performed an extensive study of DCPC oriented membrane stacks as a function of the relative humidity (RH) and at different D_2O/H_2O contrasts. This allowed us to determine the bilayer NSLD profile and to define unambiguously the phase of each of the structure factor terms F_h.

From that, and by using deuterium labelled alkanes, we found that eicosane and squalane are inserted inside the model membrane in the hydrocarbon region. At least a significate portion of the alkane molecules inserts perpendicular to the lipid chains, causing a small but significant increase in the bilayer thickness d_b, consistent with a confined elongated position of the compound in the mid-plane. The membrane swelling induced by the increase in humidity causes, on one hand, an increase of the intermembrane water thickness (as expected), while on the other hand it leads to a slight decrease in the bilayer thickness, which can be explained by a concomitant volume increase of the lipid headgroup upon hydration. The decrease of d_{HH} is not affected by the eicosane or squalane presence inside the membrane.

The sample containing the longer linear hydrocarbon alkane triacontane does not show any increase in the bilayer thickness. This, together with physical considerations about the alkane and lipid molecule sizes, implies that the triacontane molecules do not incorporate into the membrane, unlike eicosane and squalane. This is consistent with the selective exclusion of triacontane (and inclusion of squalane) molecules that has been reported in a former study with different membrane compositions [19]. The slight differences in osmotic pressure decay with water thickness d_w, indicate that the eicosane and squalane may decrease the membrane maximum swelling limit of the membrane.

Therefore, the incorporation of certain alkanes within short chain lipid membranes could have also occurred in an origin of life scenario, where both these alkanes and membrane-forming SCA could have been synthesized abiotically. This membrane enrichment, coupled with the existence of a preferential structural arrangement of the n-alkanes in the hydrophobic core, can effectively increase the membrane thickness and possibly lead to a lower membrane swelling capability. Together with previously observed effects in increasing the membrane thermal and pressure stability [21], the results suggest a role of the n-alkanes in modifying significantly the membrane structural and functional properties, constituting one of the possible survival strategies against the extreme prebiotic environmental conditions for the first membrane compartments at the origin of life.

Acknowledgements

LM was supported by a scholarship from the Institut Laue - Langevin (ILL) PhD program. The authors thank ILL for neutron beamtime on D16 (DOI: 10.5291/ILL-DATA.9-13-758 and 10.5291/ILL-DATA.9-13-906). The ILL Partnership for Soft Condensed Matter (PSCM) is acknowledged for the access to the lab infrastructures.

References

[1] J.W. Szostak, D.P. Bartel, P.L. Luisi, Synthesizing life, Nature, 409 (2001) 387-390.
[2] D. Segre, D. Ben-Eli, D.W. Deamer, D. Lancet, The lipid world, Orig Life Evol Biosph, 31 (2001) 119-145.
[3] P.L. Luisi, P. Walde, T. Oberholzer, Lipid vesicles as possible intermediates in the origin of life, Curr. Opin. Coll. Inter. Sci., 4 (1999) 33 - 39.
[4] D. Deamer, The Role of Lipid Membranes in Life's Origin, Life (Basel), 7 (2017).
[5] M. Fiore, P. Strazewski, Prebiotic Lipidic Amphiphiles and Condensing Agents on the Early Earth, Life (Basel), 6 (2016).
[6] O.G. Mouritsen, Life - As a Matter of Fat, The Frontiers Collection, Place Published, 2005.
[7] G. Zaccai, J.K. Blasie, B.P. Schoenborn, Neutron diffraction studies on the location of water in lecithin bilayer model membranes, Proc Natl Acad Sci U S A, 72 (1975) 376-380.
[8] D.L. Worcester, N.P. Franks, Structural analysis of hydrated egg lecithin and cholesterol bilayers II. Neutron diffraction, J. Mol. Biol., 3 (1976) 359 - 378.
[9] N.P. Franks, W.R. Lieb, The structure of lipid bilayers and the effects of general anaesthetics: an x-ray and neutron diffraction study, J. Mol. Biol., 134 (1979) 469 - 500.
[10] G. Büldt, H.U. Gally, J. Seelig, G. Zaccai, Neutron diffraction studies on phosphatidylcholine model membranes: I. Head group conformation, J. Mol. Biol., 134 (1979) 673 - 691.
[11] J.F. Nagle, S. Tristram-Nagle, Structure of lipid bilayers, Biochim Biophys Acta, 1469 (2000) 159-195.

[12] N. Kucerka, Y. Liu, N. Chu, H.I. Petrache, S. Tristram-Nagle, J.F. Nagle, Structure of Fully Hydrated Fluid Phase DMPC and DLPC Lipid Bilayers Using X-Ray Scattering from Oriented Multilamellar Arrays and from Unilamellar Vesicles, Biophys. J., 88 (2005) 2626-2637.
[13] N. Kucerka, S. Tristram-Nagle, J.F. Nagle, Structure of Fully Hydrated Fluid Phase Lipid Bilayers with Monounsaturated Chains, J. Membr. Biol., 208 (2006) 193 - 202.
[14] D.A. Haydon, B.M. Hendry, S.R. Levinson, J. Requena, Anaesthesia by the n-alkanes. A comparative study of nerve impulse blockage and the properties of black lipid bilayer membranes, BBA - Biomembranes, 470 (1977) 17 - 34.
[15] D.A. Haydon, B.M. Hendry, S.R. Lenvinson, J. Requena, The molecular mechanisms of anaesthesia, Nature, 268 (1977) 356 - 358.
[16] S.H. White, G.I. King, J.E. Cain, Location of hexane in lipid bilayers determined by neutron diffraction, Nature, 290 (1981) 161 - 163.
[17] T.J. McIntosh, S.A. Simon, R.C. MacDonald, The organization of n-alkanes in lipid bilayers, BBA - Biomembranes, 597 (1980) 445 - 463.
[18] T. Hauss, S. Dante, N.A. Dencher, T.H. Haines, Squalane is in the midplane of the lipid bilayer: implications for its function as a proton permeability barrier, BBA - Bioenergetics, 1556 (2002) 149 - 154.
[19] M. Salvador-Castell, B. Deme, P. Oger, J. Peters, Lipid Phase Separation Induced by the Apolar Polyisoprenoid Squalane Demonstrates Its Role in Membrane Domain Formation in Archaeal Membranes, Langmuir, 36 (2020) 7375-7382.
[20] A. Cario, V. Grossi, P. Schaeffer, P.M. Oger, Membrane homeoviscous adaptation in the piezo-hyperthermophilic archaeon Thermococcus barophilus, Frontiers in Microbiology, 6 (2015).
[21] L. Misuraca, B. Demé, P. Oger, J. Peters, Alkanes increase the stability of early life membrane models under extreme pressure and temperature conditions, Communications Chemistry, 4 (2021) 24, 21 - 28.
[22] T.M. McCollom, G. Ritter, B.R. Simoneit, Lipid synthesis under hydrothermal conditions by Fischer-Tropsch-type reactions, Orig Life Evol Biosph, 29 (1999) 153-166.
[23] B.R.T. Simoneit, Prebiotic organic synthesis under hydrothermal conditions: an overview, Advances in Space Research, 33 (2004) 88 - 94.
[24] N. Kucerka, M.P. Nieh, J. Katsaras, Fluid phase lipid areas and bilayer thicknesses of commonly used phosphatidylcholines as a function of temperature, Biochim Biophys Acta, 1808 (2011) 2761-2771.
[25] L. Misuraca, A. Calio, I. Grillo, A. Grelard, P.M. Oger, J. Peters, B. Demé, High-Temperature Behavior of Early Life Membrane Models, Langmuir, 36 (2020) 13516-13526.
[26] S. Tristram-Nagle, R. Zhang, R.M. Suter, C.R. Worthington, W.J. Sun, J.F. Nagle, Measurement of chain tilt angle in fully hydrated bilayers of gel phase lecithins, Biophys J, 64 (1993) 1097-1109.
[27] V. Cristiglio, B. Giroud, L. Didier, B. Demé, D16 is back to business: More neutrons, more space, more fun, Neutron News, 26 (2015) 22 - 24.
[28] J. Gonthier, M.A. Barrett, O. Aquettaz, S. Baudoin, E. Bourgeat-Lami, B. Demé, N. Grimm, T. Hauss, K. Kiefer, E. Lelièvre-Berna, A. Perkins, D. Wallacher, BerILL: The ultimate humidity chamber for neutron scattering, J. Neutron Res., 21 (2019) 65 - 76.
[29] D. Richard, M. Ferrand, G.J. Kearley, Analysis and visualisation of neutron-scattering data, Journal of Neutron Research, 4 (1996) 33-39.
[30] N. Kucerka, M.P. Nieh, J. Pencer, J.N. Sachs, J. Katsaras, What determines the thickness of a biological membrane, Gen Physiol Biophys, 28 (2009) 117-125.
[31] M. Kanduc, A. Schlaich, A.H. de Vries, J. Jouhet, E. Marechal, B. Deme, R.R. Netz, E. Schneck, Tight cohesion between glycolipid membranes results from balanced water-headgroup interactions, Nat Commun, 8 (2017) 14899.
[32] A.R. Denninger, B. Deme, V. Cristiglio, G. LeDuc, W.B. Feller, D.A. Kirschner, Neutron scattering from myelin revisited: bilayer asymmetry and water-exchange kinetics, Acta Crystallogr D Biol Crystallogr, 70 (2014) 3198-3211.

543 [33] D. Marquardt, F.A. Heberle, J.D. Nickels, G. Pabst, J. Katsaras, On scattered waves and lipid
544 domains: detecting membrane rafts with X-rays and neutrons, Soft Matter, 11 (2015) 9055-9072.
545 [34] https://www.ncnr.nist.gov/resources/activation/
546 [35] D.M. LeNeveu, R.P. Rand, V.A. Parsegian, Measurement of forces between lecithin bilayers,
547 Nature, 259 (1976) 601-603.
548 [36] V.A. Parsegian, N. Fuller, R.P. Rand, Measured work of deformation and repulsion of lecithin
549 bilayers, Proc. Natl. Acad. Sci. USA, 76 (1979) 2750 - 2754.
550 [37] E. Sparr, H. Wennerstrom, Responding phospholipid membranes--interplay between hydration
551 and permeability, Biophys J, 81 (2001) 1014-1028.
552 [38] M. Salvador-Castell, M. Golub, N. Erwin, B. Demé, N.J. Brooks, R. Winter, J. Peters, P.M. Oger,
553 Characterisation of a synthetic Archeal membrane reveals a possible new adaptation route to
554 extreme conditions, Commun Biol, 4 (2021) 653.
555 [39] L. Misuraca, A. Calio, J.G. LoRicco, I. Hoffman, R. Winter, B. Demé, J. Peters, P.M. Oger, Alkanes
556 as membrane regulators of the response of early membranes to extreme temperatures, Life, (2022)
557 accepted for publication.
558 [40] L. Misuraca, A. Calio, J.G. LoRicco, I. Hoffman, R. Winter, B. Demé, J. Peters, P.M. Oger, Alkanes
559 as Membrane Regulators of the Response of Early Membranes to Extreme Temperatures, life, 12
560 (2022) 445, 441 - 447.
561 [41] L. Misuraca, T. Matsuo, A. Cisse, J. LoRicco, A. Calio, J.M. Zanotti, B. Deme, P. Oger, J. Peters,
562 High temperature molecular motions within a model protomembrane architecture, Phys Chem
563 Chem Phys, (2022).

564